International Journal of Heat and Fluid Flow 30 (2009) 1157–1170

Contents lists available at ScienceDirect

International Journal of Heat and Fluid Flow

journal homepage: www.elsevier.com/locate/ijhff

Scaling for unsteady thermo-magnetic convection boundary layer of paramagnetic fluids of $Pr > 1$ in micro-gravity conditions

Tomasz P. Bednarz [a,b,*], Wenxian Lin [b], John C. Patterson [b,d], Chengwang Lei [b,d], Steven W. Armfield [c]

[a] CSIRO Division of Exploration and Mining, QCAT, Technology Court, Pullenvale QLD 4069, Australia
[b] School of Engineering and Physical Sciences, James Cook University, Townsville, QLD 4811, Australia
[c] School of Aerospace, Mechanical and Mechatronic Engineering, The University of Sydney, NSW 2006, Australia
[d] School of Civil Engineering, The University of Sydney, NSW 2006, Australia

ARTICLE INFO

Article history:
Received 24 December 2008
Received in revised form 21 August 2009
Accepted 30 August 2009
Available online 2 October 2009

Keywords:
Magnetic convection
Magneto-thermal convection
Boundary layer
Unsteady flow
Paramagnetic fluid
Prandtl number

ABSTRACT

This work incorporates scaling analysis to characterise unsteady boundary-layer development for thermo-magnetic convection of paramagnetic fluids with Prandtl numbers (Pr) greater than one. Under consideration is a square cavity with a quiescent isothermal, Newtonian fluid placed in a micro-gravity condition ($g \approx 0$), and under a uniform vertical gradient magnetic field. A distinct magnetic convection boundary layer is produced by the sudden imposition of a higher temperature on the left-hand side vertical sidewall due to the effect of the magnetic body force generated on the paramagnetic fluid. This magnetic force is proportional to the magnetic susceptibility and the gradient of the square of the magnetic induction. According to Curie's law, the magnetic susceptibility of a paramagnetic fluid is inversely proportional to the absolute temperature. Thermal convection of a paramagnetic fluid can therefore take place even in zero-gravity environments as a direct consequence of temperature differences occurring within the fluid placed within a magnetic field gradient.

Scaling predictions presented here are verified by numerical simulations It is shown that the transient flow behaviour of the resulting boundary layer can be described by three stages: a start-up stage, a transitional stage and a steady state. Special attention in this work is paid to the dependency of the flow development upon the Prandtl number, varied over the range of 5–100, thus representing various fluids. Also, the effect of the magnetic momentum parameter, m, and the quantity γRa, upon the flow development obtained in numerical simulations confirms the accuracy of new scaling predictions for paramagnetic fluids.

Crown Copyright © 2009 Published by Elsevier Inc. All rights reserved.

1. Introduction

Natural convection in a gravitational field is ubiquitous in nature and in many practical settings. Its importance in oceanography, geophysics, meteorology, astrophysics, energy systems, material science, etc. is reflected by extensive studies using analytical, experimental and numerical means. Transient convection flow behaviour is a class of flows of that has been of fundamental interest in fluid mechanics and practical applications. The simplest and classical example of convective flow in terrestrial conditions is the heating of a relatively cold fluid in a cavity by imposing a higher temperature on the vertical sidewalls. The fluid adjacent to the wall undergoes motion as a result of heat being transferred from the wall into the fluid. The warmer fluid becomes less dense and rises relative to the ambient colder fluid. Patterson and Imberger (1980) used scaling analysis to predict the transient flow behaviour in a two-dimensional rectangular cavity when two opposite vertical sidewalls were heated and cooled simultaneously with the same amount of heating applied. With their scaling analysis technique, they were able to perform a classification of the flow development through several transient flow regimes based on the governing parameters of the flow; the Rayleigh number, Ra, the Prandtl number, Pr, and the aspect ratio of the cavity, A. Since then, extensive investigations have been conducted for many aspects of unsteady natural convection boundary-layer flow under various flow configurations through the use of scaling analysis, numerical simulations and experiments, as recently reviewed by Lin et al. (2007). In particular, scaling analysis has been used to accurately predict the Ra and A dependence of the transient natural convection flow behaviour under various flow configurations (Armfield et al., 2007; Lin et al., 2008, 2002; Lin and Armfield, 1999, 2005). Nevertheless, it has also been shown that some of the scalings obtained from scaling analysis do not perform satisfactorily with Pr

* Corresponding author. Address: CSIRO Division of Exploration and Mining, QCAT, Technology Court, Pullenvale QLD 4069, Australia. Tel.: +61 7 3327 4706; fax: +61 7 3327 4566.
E-mail address: tomasz.bednarz@csiro.au (T.P. Bednarz).

0142-727X/$ - see front matter Crown Copyright © 2009 Published by Elsevier Inc. All rights reserved.
doi:10.1016/j.ijheatfluidflow.2009.08.003

variation. This prompted researchers to develop improved scalings by taking into account *Pr* variation in the scaling analysis. Recently, Patterson et al. (2009) and Lin et al. (2009) carried out improved scaling analyses for the unsteady natural convection boundary layers of fluids with $Pr > 1$ placed under ramped and instantaneous isothermal heating conditions, respectively. Aberra et al. (2008) carried out a similar study for the steady-state natural convection boundary layers of fluids with $Pr > 1$ under isoflux heating conditions. In this study, the improved scaling analysis was extended to predict the transient magnetic convection boundary layer in a micro-gravity environment.

In a micro-gravity environment, there is no gravitational buoyancy acting on the fluid and natural convection phenomena are not present. However, if the fluid itself is subject to a magnetic field, it will experience a magnetic force, which strongly depends upon whether the fluid considered is diamagnetic, paramagnetic or ferromagnetic. The present work considers only paramagnetic fluids and hence the magnetic force depends on the magnetic susceptibility and the gradient of the square of magnetic induction. Additionally, magnetic susceptibility depends on the absolute temperature according to Curie's law. As will be shown in Section 2, if there is a temperature difference in the fluid, a magnetic buoyancy force will be present. This will be the main driving force for a convective flow (magnetic convection) even if there is no gravity acting on the system. It is only a relatively recent fact, with the advent of super-conducting magnets, that magnetic convection can be studied on Earth (i.e. not in micro-gravity environments such as orbiting laboratories). There are huge benefits behind investigations of these new topics. The most important one is the possibility of control of the convection phenomena and heat transfer rates in a terrestrial environment. In Braithwaite et al. (1991) reported enhancement or cancellation of gravitational convection due to a magnetic field for a solution of gadolinium nitrate in a shallow layer heated from below and cooled from above. Ozoe and his coworkers have studied the effects of magnetic fields on various convective phenomena (Ozoe, 2005). Tagawa et al. (2002, 2003) derived a model equation for magnetic convection using a method similar to the Boussinesq approximation and carried out numerical simulations in a cubic cavity. Bednarz et al. (2004, 2005a,b, 2006, 2008, 2009) have shown both numerically and experimentally how to enhance or suppress heat transfer by the application of a magnetic field. Their various experiments and numerical simulations for varied position of the magnet relative to the experimental enclosure together with investigations of the magnetic convection of paramagnetic materials have verified the modelling approaches used in those studies. Kaneda et al. (2002) have also studied the effect of a gradient magnetic field with a four-pole electric magnet. They placed a cubic enclosure filled with air inside the magnetic field and heated the air from above and cooled it from below at the center of the four-pole magnet. The stagnant conduction of air in the cube was disturbed and the convection of air was visualized with incense smoke, which was injected downwards from the center of the hot top plate toward the cold bottom plate, opposing the gravitational buoyancy force. This peculiar behaviour of air agreed well with their corresponding numerical analysis. More information about magnetic convection and its application can be found in the recent book of Ozoe (2005).

This present work extends previous investigations on magnetic convection of paramagnetic fluids, focusing on the transient behaviour and predictions of the boundary-layer development. In Section 2, the basis of the magnetic force is developed. In Section 3, the full equations are formulated, and in Section 4, a scaling analysis is described. Section 5 presents the resulting scales in dimensionless forms. The numerical method is described in Section 6, and the validation of the scales by the numerical results is carried out in Section 7. Final conclusions are drawn in Section 8.

2. The magnetic buoyancy force

The magnetic body force $\vec{f}_m$ is given in the following form (Carruthers and Wolfe, 1968; Chandrasekhar, 1981; Bai et al., 1999):

$$\vec{f}_m = \frac{\mu_m \chi \rho}{2} \vec{\nabla} H^2, \quad H^2 = \vec{H} \cdot \vec{H} \tag{1}$$

where μ_m is the magnetic permeability [H/m], χ the magnetic susceptibility [m^3/kg], ρ the density of the fluid [kg/m^3], and $\vec{H}$ is the magnetic field strength [A/m].

Using the following relationship between the magnetic field strength $\vec{H}$ and the magnetic induction $\vec{b}$ [T = Wb/m^2 = V s/m^2]

$$\vec{b} = \mu_m (1 + \chi \rho) \vec{H}, \tag{2}$$

the magnetic body force can be approximated as:

$$\vec{f}_m = \frac{\mu_m \chi \rho}{2} \vec{\nabla} \left[\frac{b^2}{\mu_m^2 (1 + \chi \rho)^2} \right] \cong \frac{\chi \rho}{2 \mu_m} \vec{\nabla} b^2 \tag{3}$$

under the assumption $\chi \rho \ll 1$. Table 1 lists the mass and volumetric susceptibilities of some common paramagnetic materials measured at room temperature, clearly demonstrating this validity of this assumption for common electrically non-conducting paramagnetic materials.

The magnetic body force (3) can be included in the Navier–Stokes equation as an external force as follows:

$$\rho \frac{D\vec{u}}{Dt} = -\vec{\nabla} p + \mu \nabla^2 \vec{u} + \frac{\chi \rho}{2 \mu_m} \vec{\nabla} b^2 \tag{4}$$

where t is the time [s], $\vec{u}$ the velocity vector [m/s], p the pressure [N/m^2], and μ is the viscosity of the fluid [Pa s].

The magnetic force term is proportional to the gradient of the square of magnetic induction. However, when χ and ρ are constant, convection does not occur. Assuming this state is represented by $\rho = \rho_0$, $p = p_0$ and $\vec{u} = 0$, Eq. (4) gives:

$$0 = -\vec{\nabla} p_0 + \frac{\chi_0 \rho_0}{2 \mu_m} \vec{\nabla} b^2 = \vec{\nabla} \left(-p_0 + \frac{\chi_0 \rho_0}{2 \mu_m} b^2 \right) \tag{5}$$

When a temperature difference exists, the magnetic susceptibility and density change with temperature. Pressure p can therefore be expressed as the summation of a perturbed pressure p' and the static pressure p_0:

$$p = p_0 + p' \tag{6}$$

The difference between Eqs. (4) and (5) is:

$$\frac{D\vec{u}}{Dt} = -\frac{1}{\rho} \vec{\nabla} p' + \nu \nabla^2 \vec{u} + \frac{1}{2 \mu_m} \left(\chi - \chi_0 \frac{\rho_0}{\rho} \right) \vec{\nabla} b^2 \tag{7}$$

According to Curie's law, the magnetic susceptibility of paramagnetic fluids is related to temperature T [K] as follows,

$$\chi = \frac{C}{T} \tag{8}$$

Table 1
Magnetic susceptibilities of some common paramagnetic materials at the room temperature (CRC Handbook of Chemistry, 2007).

Material	Volumetric susceptibility χ_m [−] ($\times 10^{-6}$)	Mass susceptibility χ [m^3/kg] ($\times 10^{-8}$)
Oxygen (gas O_2)	1.772	135.447
Sodium (Na)	8.483	0.875
Aluminium (Al)	20.749	0.768
Tungsten (W)	69.920	0.362
Niobium (Nb)	239.982	2.813
Uranium (U)	412.417	2.216

where C is a constant, which leads to

$$\frac{\partial \chi}{\partial T} = \frac{\partial}{\partial T}\left(\frac{C}{T}\right) = -\frac{C}{T^2} = -\frac{\chi}{T} \tag{9}$$

When the temperature difference within the fluid is small, magnetic susceptibility can be approximated by a Taylor expansion as follows:

$$\chi \approx \chi_0 + \left[\frac{\partial \chi}{\partial T}\right]_0 (T - T_0) \tag{10}$$

and

$$\frac{1}{\rho} = \frac{1}{\rho_0[1-\beta(T-T_0)]} \approx \frac{1}{\rho_0}[1+\beta(T-T_0)] \tag{11}$$

Hence, the momentum Eq. (7) becomes:

$$\frac{D\vec{u}}{Dt} = -\frac{1}{\rho}\vec{\nabla}p' + \nu\nabla^2\vec{u} - \frac{\chi_0(\beta + 1/T_0)}{2\mu_m}(T-T_0)\vec{\nabla}b^2 \tag{12}$$

From this equation, it is seen that the magnetic buoyancy term depends on the gradient of the square of the magnetic induction and is driven by temperature variations.

3. Governing equations and system considered

The governing equations of motion for electrically non-conducting paramagnetic thermo-fluids subject to a magnetic field, together with the temperature equation, can be written in the following two-dimensional form:

$$\frac{\partial u}{\partial x} + \frac{\partial v}{\partial y} = 0 \tag{13}$$

$$\frac{\partial u}{\partial t} + u\frac{\partial u}{\partial x} + v\frac{\partial u}{\partial y} = -\frac{1}{\rho_0}\frac{\partial p}{\partial x} + \nu\left(\frac{\partial^2 u}{\partial x^2} + \frac{\partial^2 u}{\partial y^2}\right) - \frac{\chi_0(\beta + 1/T_0)}{2\mu_m}(T-T_0)\frac{\partial (b^2)}{\partial x} \tag{14}$$

$$\frac{\partial v}{\partial t} + u\frac{\partial v}{\partial x} + v\frac{\partial v}{\partial y} = -\frac{1}{\rho_0}\frac{\partial p}{\partial y} + \nu\left(\frac{\partial^2 v}{\partial x^2} + \frac{\partial^2 v}{\partial y^2}\right) - \frac{\chi_0(\beta + 1/T_0)}{2\mu_m}(T-T_0)\frac{\partial (b^2)}{\partial y} \tag{15}$$

$$\frac{\partial T}{\partial t} + u\frac{\partial T}{\partial x} + v\frac{\partial T}{\partial y} = \kappa\left(\frac{\partial^2 T}{\partial x^2} + \frac{\partial^2 T}{\partial y^2}\right) \tag{16}$$

where u and v are the x-direction and y-direction velocity components, t the time, p the pressure, T the temperature, and β, ν and κ are the thermal expansion coefficient, kinematic viscosity and thermal diffusivity of the fluid at T_0.

Under consideration is the transient flow behaviour resulting from heating a quiescent, isothermal Newtonian fluid with $Pr > 1$ in a two-dimensional open cavity of height H by imposing a fixed higher temperature, T_w, on the left-hand side vertical sidewall, in the absence of gravity but in the presence of a magnetic field, as shown in Fig. 1. The fluid is initially at rest and at a uniform temperature T_0 ($T_0 < T_w$). The heat transferred by conduction through the sidewall leads to an increase in the temperature of the fluid adjacent to the wall which changes the magnetic susceptibility of the paramagnetic fluid, resulting in a magnetic buoyancy force within the fluid. It is this magnetic buoyancy force, in the presence of a magnetic field, that acts as the driving force for the resultant magnetic convection. The top and the bottom walls are kept adiabatic and the right-hand side boundary is open, where the first

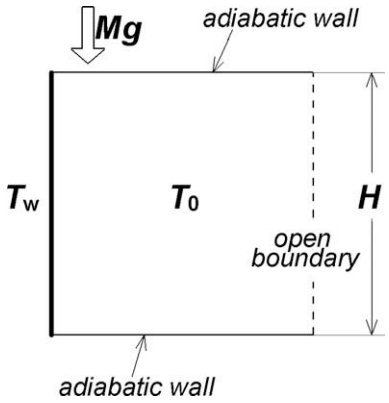

Fig. 1. Schematic of the physical system under consideration. T_w is the hot wall temperature, T_0 is the temperature of the fluid at $t \leqslant 0$.

derivatives of temperature, velocities, and pressure are all assumed to be zero. All boundaries except the right-hand boundary are non-slip. It is also assumed that the flow is laminar. The fluid is assumed to be subject to a uniform, vertical gradient magnetic field (i.e., it is assumed that $\frac{\partial(b^2)}{\partial x} = 0, \frac{\partial(b^2)}{\partial y} = \text{constant}$). Using the assumption for the vertical gradient magnetic field, the problem becomes similar to the transient gravitational natural convection flow in a differentially heated cavity. It has been demonstrated previously that two-dimensional numerical simulations characterise well such phenomena (Patterson and Armfield, 1990). In reality however, the magnetic field gradient can be more complex and therefore three-dimensional modelling may be necessary in future investigations. The present results show the simplified two-dimensional model, which becomes an entry point for more complex, further research on scaling and analysis of magnetic convection. Examples of numerical simulations in a three-dimensional cube can be found in our previous works (Bednarz et al., 2004, 2005a,b, 2006, 2008, 2009).

For natural convection flow without the magnetic effect, the transient flow behaviour is generally characterised by Pr and Ra (see, e.g. Patterson and Imberger, 1980; Lin et al., 2007), where Pr characterises the ratio of momentum diffusion to thermal diffusion, and Ra characterises the ratio of buoyancy to viscous forces and therefore the relative strength of the thermal forcing. Pr and Ra are defined as follows,

$$Pr = \frac{\nu}{\kappa}, \quad Ra = \frac{g\beta\Delta T H^3}{\nu\kappa} \tag{17}$$

For a natural convection flow with the magnetic effect, the transient flow behaviour is also characterised by an additional parameter, γ (see, e.g. Tagawa et al., 2002; Bednarz et al., 2006), which describes the strength of the magnetic forcing acting on the system, and is defined as:

$$\gamma = \frac{\chi_0 b_0^2}{\mu_m g H} \tag{18}$$

Nevertheless, if only micro-gravity magneto-thermal convection conditions are considered (i.e., $g \approx 0$, as is the case considered here), Ra becomes zero and γ becomes infinity. In this case, their product becomes finite and is herein nominated as the appropriate parameter to characterise the magnetic effect (Bednarz et al., 2005b, 2004):

$$\gamma Ra = \frac{\chi_0 b_0^2 \beta \Delta T H^2}{\mu_m \nu \kappa} \tag{19}$$

A typical flow development of the thermal boundary layer is illustrated in Fig. 2, where numerically simulated temperature contours are shown for the specific case of $\gamma Ra = 10^7$ and $Pr = 10$

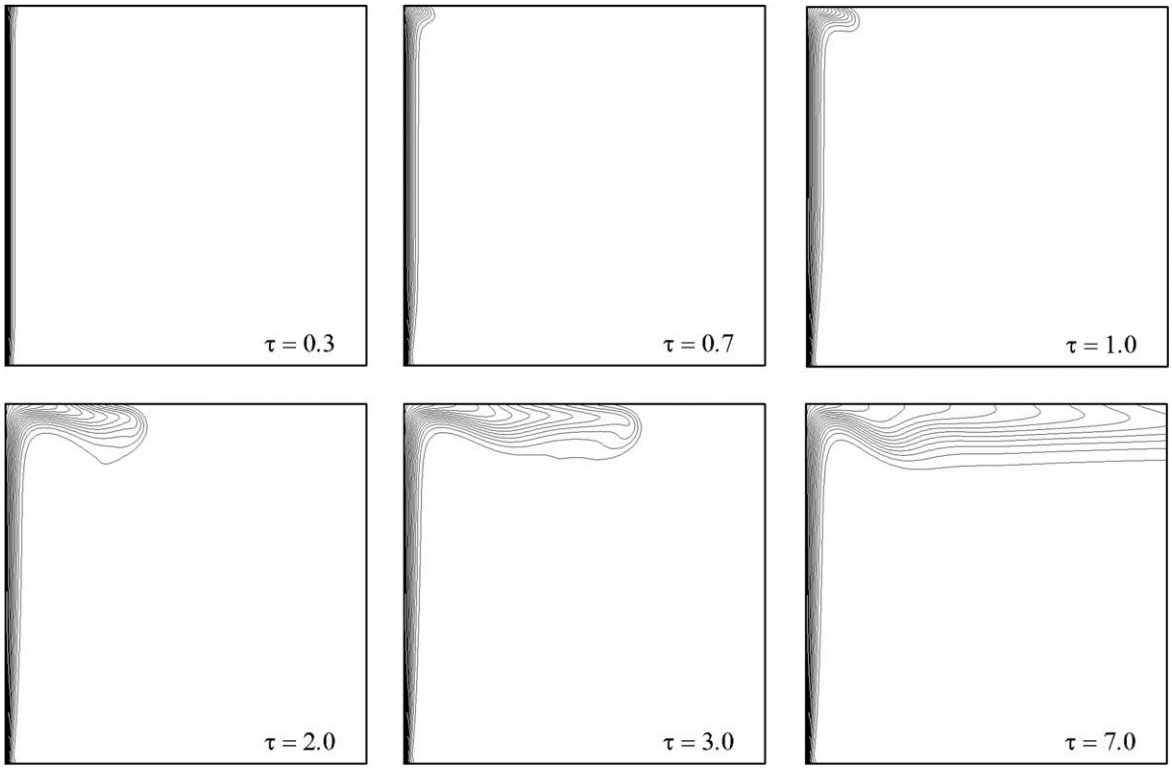

Fig. 2. Numerically simulated temperature contours at the start-up stage (top row) and the steady state (bottom row) of the boundary-layer development at $\gamma Ra = 10^7$, $Pr = 10$ and $m = 2$ (Case 2), where τ is the time normalised by H/v_0.

Table 2
Values of γRa, Pr, m for 10 simulation runs.

Run number	γRa	Pr	m
1	10^6	10	2
2	10^7	10	2
3	10^8	10	2
4	10^9	10	2
5	10^7	5	2
6	10^7	20	2
7	10^7	50	2
8	10^7	100	2
9	10^7	10	1
10	10^7	10	5

(Case 2 listed in Table 2). In this case, the boundary layer becomes fully developed at $\tau \approx 3$, where τ is the dimensionless time defined later in Section 5. The heated fluid that ejects from the boundary-layer flows along the top wall toward right-hand side open boundary. In the next sections, scaling relations will be developed for the relevant parameters characterising the flow behaviour at different flow stages.

4. Scaling analysis

In the early stage of flow development, a boundary layer adjacent to the heated wall is developed. The flow experiences a start-up stage dominated by one-dimensional conduction that is perpendicular to the left-hand side vertical wall, followed by a short transitional stage during which one-dimensional conduction transits to a two-dimensional magneto-thermal convection, before reaching a steady-state stage. Obviously, the effect of the wall is restricted to a thin layer close to the wall, since the additional energy supplied to the fluid through the wall is transported up or down along the wall by convection (depending on the sign of the vertical gradient of the square of magnetic induction) and thus cannot reach regions of fluid further away from the wall.

The following parameters characterise the flow behaviour at the boundary-layer development stage: δ_T – the thermal boundary layer thickness, v_m – the y-direction maximum velocity within the boundary layer, t_s – the time for the boundary layer to reach the steady state, Nu_y – the local Nusselt number at height y and Nu – the global Nusselt number along the whole vertical sidewall, respectively. δ_T is defined as the distance in the x-direction between the vertical sidewall and the location where $(T-T_0)$ becomes $0.01(T_w-T_0)$. This thickness grows with the length y and derives from a simple energy balance, namely, the total energy supplied through the wall up to a point y must "flow" by convection of the higher temperature fluid over the cross-section y = const (Schlichting and Gersten, 2000). Therefore, the time t_s for the boundary-layer development to reach the steady state is determined as the moment when δ_T ceases to change with time.

4.1. Start-up stage

Initially, heat is transferred to the fluid body by pure conduction which results in a one-dimensional vertical thermal boundary layer. Comparing the magnitudes of the unsteady term $O(\Delta T/t)$ with the convective term $O(v\Delta T/H)$ in the energy Eq. (16) gives the following relation,

$$\frac{\text{unsteady term}}{\text{convection term}} \sim \frac{\Delta T/t}{v\Delta T/H} \sim \frac{H}{vt} \tag{20}$$

For sufficiently small t, this ratio becomes much larger than 1, and therefore the initial balance in (16) is between the heat conducted in though the wall, i.e., $O(\kappa\Delta T/\delta_T^2)$, and the unsteady term,

$$\frac{\Delta T}{t} \sim \kappa \frac{\Delta T}{\delta_T^2} \tag{21}$$

which leads to the following scaling for δ_T at the start-up stage:

$$\delta_T \sim \kappa^{0.5} t^{0.5} \tag{22}$$

Hence, the gradient of the temperature exists from the wall to a distance δ_T.

The magnetic buoyancy force results from conductive heating, acting to accelerate the flow over the thickness δ_T only. In this region the ratio of the inertial term, $O(v/t)$, and the viscous term $O(v\, v/\delta_T^2)$ in the y-directional momentum Eq. (15), is:

$$\frac{\text{inertial term}}{\text{viscous term}} \sim \frac{v/t}{v\, v/\delta_T^2} \sim \frac{\delta_T^2}{vt} \sim \frac{1}{\text{Pr}} \tag{23}$$

For $Pr \gg 1$, this ratio becomes much smaller than 1, and therefore the balance over δ_T is between the viscous term and the magnetic buoyancy term,

$$0 \sim v \frac{\partial^2 v}{\partial x^2} - \frac{\chi_0(\beta + 1/T_0)}{2\mu_m} \Delta T \frac{\partial(b^2)}{\partial y} \tag{24}$$

Following the arguments of Patterson et al. (2009) and Lin et al. (2009), Fig. 3 shows a three-region structure for magnetic convection boundary layers for $Pr > 1$. The peak velocity v_m occurs within the thermal boundary layer δ_T at a distance δ_{vm} from the wall. Also, there will be a region of flow outside δ_T where the flow is not directly forced by buoyancy, but is instead the result of diffusion of momentum via viscosity. This occurs up to a distance δ_v from the wall.

In regions I and II, the balance is between viscosity and buoyancy. However, in region III the balance is between viscosity and inertia, since there is no buoyancy there.

In region I, the balance (24) gives:

$$v \frac{v_m}{\delta_{vm}^2} \sim \frac{\chi_0(\beta + 1/T_0)\, \Delta T}{\mu_m} \frac{\partial(b^2)}{\partial y}, \tag{25}$$

thus:

$$v_m \sim \frac{\chi_0(\beta + 1/T_0)\, \Delta T}{\mu_m v} \delta_{vm}^2 \frac{\partial(b^2)}{\partial y}, \tag{26}$$

In region II, the forcing is over distance $(\delta_T - \delta_{vm})$, but the gradient of the velocity is over $(\delta_v - \delta_{vm})$. Therefore, a suitable scaling analysis would be to integrate relation (24) over region II:

$$0 \sim v \left(\frac{\partial v}{\partial x}\right)_{\delta_{vm}}^{\delta_v} - \frac{\chi_0(\beta + 1/T_0)}{\mu_m} \frac{\partial(b^2)}{\partial y} \int_{\delta_{vm}}^{\delta_T} T dx. \tag{27}$$

Since, at the maximum $(\partial v/\partial x)_{\delta_{vm}} = 0$ and $\int_{\delta_{vm}}^{\delta_T} T dx \sim \Delta T(\delta_T - \delta_{vm})$, this gives:

$$v \frac{v_m}{\delta_v - \delta_{vm}} \sim \frac{\chi_0(\beta + 1/T_0)\Delta T}{\mu_m} \frac{\partial(b^2)}{\partial y} (\delta_T - \delta_{vm}). \tag{28}$$

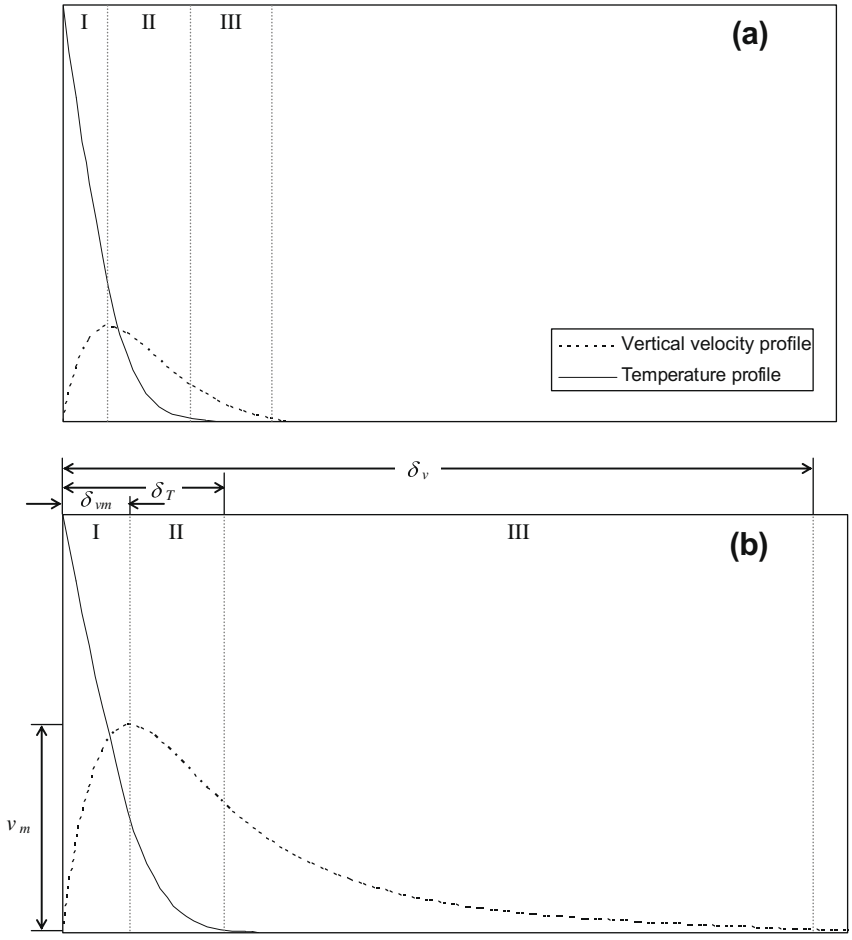

Fig. 3. Numerically simulated horizontal profiles of vertical velocity and temperature at height $Y = 0.5$ within the boundary layer: (a) at the start-up stage (at time $\tau = 0.5$) and (b) at steady state (at time $\tau = 25$) for $Ra = 10^7$, $Pr = 10$, and $m = 2$ (Case 2), where τ and Y are dimensionless time and height defined by H/v_0 and y/H.

Hence,

$$v_m \sim \frac{\chi_0(\beta + 1/T_0)\Delta T}{\mu_m \nu} \frac{\partial(b^2)}{\partial y}(\delta_T - \delta_{vm})(\delta_v - \delta_{vm}). \tag{29}$$

Matching this with (26), gives:

$$\delta_{vm}^2 \sim (\delta_T - \delta_{vm})(\delta_v - \delta_{vm}), \tag{30}$$

so that:

$$\delta_{vm}^2 \sim \delta_T \delta_v - (\delta_T + \delta_v)\delta_{vm} + \delta_{vm}^2, \tag{31}$$

which leads to:

$$\delta_{vm} \sim \frac{\delta_T \delta_v}{\delta_T + \delta_v}. \tag{32}$$

Finally, in region III, the flow is driven by diffusion of momentum, therefore, as mentioned above, the unsteady term balances the viscous term, giving:

$$\frac{v}{t} \sim \nu \frac{v}{\delta_v^2}. \tag{33}$$

This leads to scaling for δ_v at the start-up stage:

$$\delta_v \sim \nu^{0.5} t^{0.5} \sim Pr^{0.5} \delta_T. \tag{34}$$

Thus, the scaling (32) for δ_{vm} becomes:

$$\delta_{vm} \sim \frac{Pr^{0.5}}{1 + Pr^{0.5}} \delta_T \sim \frac{1}{1 + Pr^{-0.5}} \kappa^{0.5} t^{0.5}. \tag{35}$$

The scaling (26) for v_m can be therefore written as:

$$v_m \sim \frac{\chi_0(\beta + 1/T_0)\Delta T}{\mu_m \nu} \frac{\partial(b^2)}{\partial y} \delta_{vm}^2 \sim \frac{\chi_0(\beta + 1/T_0)\Delta T}{\mu_m \nu} \frac{\partial(b^2)}{\partial y} \left(\frac{1}{1 + Pr^{-0.5}}\right)^2 \delta_T^2, \tag{36}$$

Since $\delta_T \sim \kappa^{0.5} t^{0.5}$, the scaling (36) becomes:

$$v_m \sim \frac{\chi_0(\beta + 1/T_0)\Delta T}{\mu_m \nu} \frac{\partial(b^2)}{\partial y} \left(\frac{1}{1 + Pr^{-0.5}}\right)^2 \kappa t \sim (\gamma Ra) \frac{m\kappa^2}{H^3} \left(\frac{1}{1 + Pr^{-0.5}}\right)^2 t, \tag{37a}$$

where

$$m = 1 + \frac{1}{\beta T_0}, \tag{37b}$$

is a dimensionless momentum parameter for paramagnetic fluid (Bednarz et al., 2009; Shigemitsu et al., 2003). The meaning of the

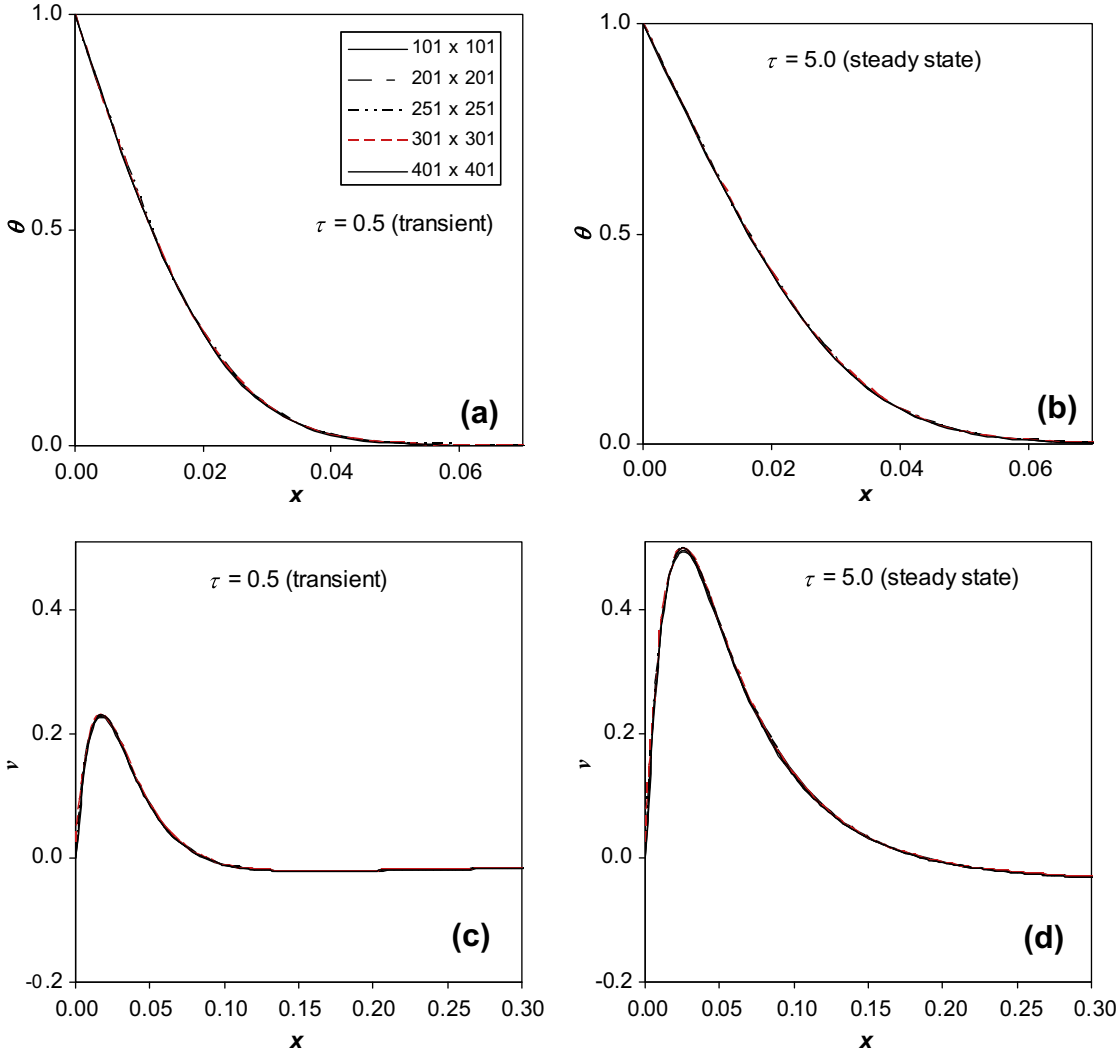

Fig. 4. Numerically simulated horizontal temperature and vertical velocity profiles at height $Y = 0.5$ for $Ra = 10^7$, $Pr = 10$, and $m = 2$ with five different meshes at transient and steady boundary-layer development stages.

parameter m should be considered as a correction factor for momentum equations when considering magnetic convection. This was verified by comparison of experimental results with numerical simulations (Bednarz et al., 2005a, 2006, 2008, 2009; Kaneda et al., 2002).

The instantaneous Nusselt number at height y on the vertical sidewall during the boundary-layer development stage is:

$$Nu_y \sim \frac{\left(\frac{\partial T}{\partial x}\right)_{x=0}}{\frac{\Delta T}{H}} \sim \frac{H}{\Delta T}\frac{\Delta T}{\delta_T} \sim \frac{H}{\kappa^{0.5} t^{0.5}}, \tag{38a}$$

and the global Nusslet number at the start-up stage is:

$$Nu = \frac{1}{H}\int_0^H Nu_y dy \tag{38b}$$

4.2. Steady state

The boundary layer continues to grow until the convection of heat carried away by the flow balances the conduction of heat transferred through the wall, which, from (16), leads to,

$$v_m \frac{\partial T}{\partial y} \sim \kappa \frac{\partial^2 T}{\partial x^2}, \tag{39}$$

At the height y, this happens when

$$v_m \frac{\Delta T}{y} \sim \kappa \frac{\Delta T}{\delta_T^2}, \tag{40}$$

i.e.

$$(\gamma Ra)\frac{m\kappa^2}{H^3 y}\left(\frac{1}{1+Pr^{-0.5}}\right)^2 t \sim \kappa \frac{1}{\kappa t}. \tag{41}$$

This leads to:

$$t^2 \sim \frac{1}{(\gamma Ra)}\frac{H^3 y}{m\kappa^2}(1+Pr^{-0.5})^2, \tag{42}$$

which gives the following scaling for the time when the boundary layer reaches steady state:

$$t_s \sim \frac{H^2}{(\gamma Ra)^{0.5} m^{0.5}\kappa}\left(\frac{y}{H}\right)^{0.5}(1+Pr^{-0.5}). \tag{43}$$

The corresponding scaling for the steady state maximum velocity, from (37), is:

$$v_{m,s} \sim (\gamma Ra)\frac{m\kappa^2}{H^3}\left(\frac{1}{1+Pr^{-0.5}}\right)^2 t_s \sim (\gamma Ra)^{0.5}\frac{m^{0.5}\kappa}{H}\left(\frac{y}{H}\right)^{0.5}\frac{1}{(1+Pr^{-0.5})}. \tag{44}$$

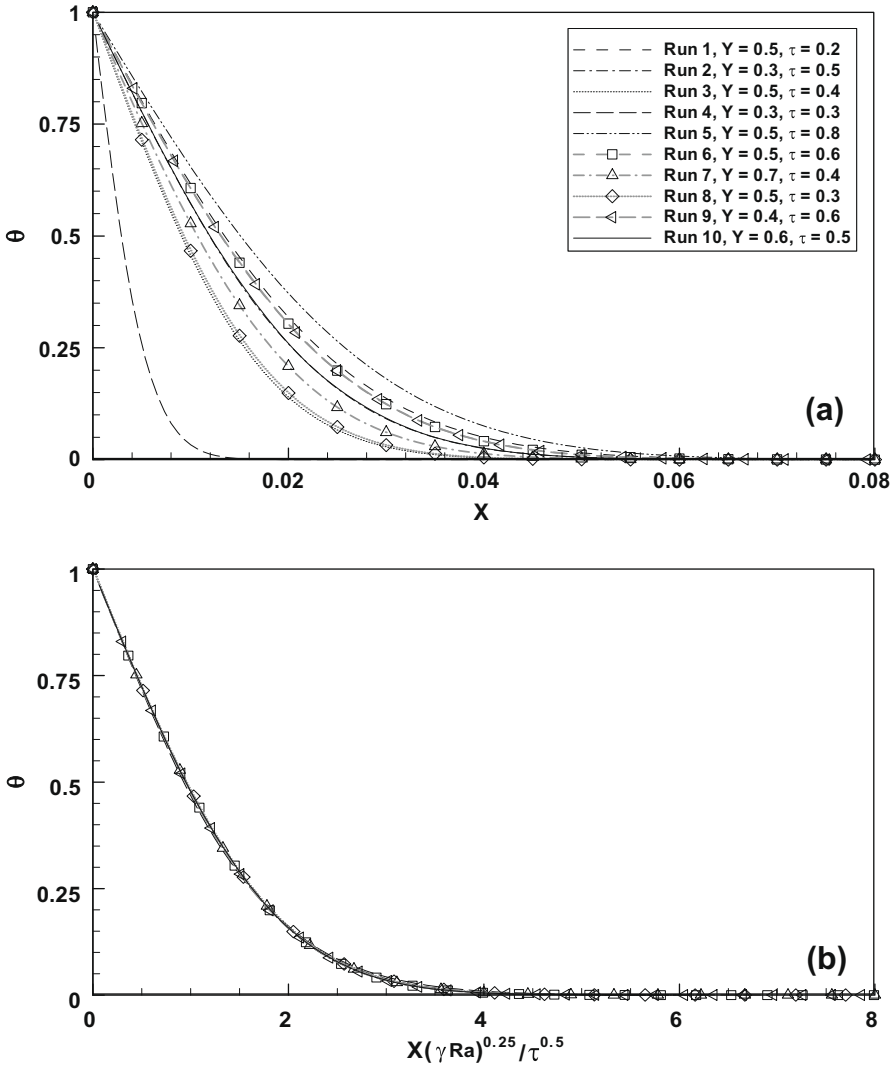

Fig. 5. Horizontal temperature profiles for all cases considered at different heights and times during the start-up stage: (a) raw data and (b) θ plotted agains $X(\gamma Ra)^{0.25}/\tau^{0.5}$.

The scaling for the steady state thermal boundary layer thickness, from (22), is

$$\delta_{T,s} \sim \kappa^{0.5} t_s^{0.5} \sim \frac{H}{(\gamma Ra)^{0.25} m^{0.25}} \left(\frac{y}{H}\right)^{0.25} (1 + Pr^{-0.5})^{0.5}. \quad (45)$$

The scaling for the steady state inner viscous boundary layer thickness, from (35), is

$$\delta_{vm,s} \sim \frac{Pr^{0.5}}{1 + Pr^{0.5}} \delta_{T,s} \sim \frac{H}{(\gamma Ra)^{0.25} m^{0.25}} \left(\frac{y}{H}\right)^{0.25} \frac{1}{(1 + Pr^{-0.5})^{0.5}}. \quad (46)$$

The scaling for the steady state whole viscous boundary layer thickness, from (34), is

$$\delta_{v,s} \sim Pr^{0.5} \delta_{T,s} \sim \frac{H}{(\gamma Ra)^{0.25} m^{0.25}} \left(\frac{y}{H}\right)^{0.25} Pr^{0.5} (1 + Pr^{-0.5})^{0.5}. \quad (47)$$

At steady state, from (43), the local Nusselt number becomes:

$$Nu_{s,y} \sim (\gamma Ra)^{0.25} m^{0.25} \left(\frac{H}{y}\right)^{0.25} \frac{1}{(1 + \mathrm{Pr}^{-0.5})^{0.5}} \quad (48)$$

The steady state global Nusselt number Nu is then given by:

$$Nu \sim \frac{1}{H} \int_0^H Nu_{s,y} dy \sim (\gamma Ra)^{0.25} m^{0.25} \frac{1}{(1 + Pr^{-0.5})^{0.5}} \quad (49)$$

5. Dimensionless formulation

To facilitate the numerical validation of the scalings obtained above, dimensionless forms of the governing equations and the scalings are used. For the magneto-thermal natural convection boundary layer considered here, it is natural to choose H, the height of the vertical sidewall, as the characteristic length scale. From (44), it is also natural to choose

$$v_0 = \frac{\kappa (\gamma Ra)^{0.5}}{H} \quad (50)$$

as the characteristic velocity scale. Hence, the characteristic time scale for the flow is apparently (H/v_0) and the characteristic pressure scale is $\rho {v_0}^2$. It is also apparent that $\Delta T = T_w - T_0$ is an appropriate temperature difference scale.

With these characteristic scales, the governing Eqs. (13)–(16) can be written in the following non-dimensional forms,

$$\frac{\partial U}{\partial X} + \frac{\partial V}{\partial Y} = 0 \quad (51)$$

$$\frac{\partial U}{\partial \tau} + U \frac{\partial U}{\partial X} + V \frac{\partial U}{\partial Y} = -\frac{\partial P}{\partial X} + \frac{Pr}{(\gamma Ra)^{0.5}} \left(\frac{\partial^2 U}{\partial X^2} + \frac{\partial^2 U}{\partial Y^2}\right) \quad (52)$$

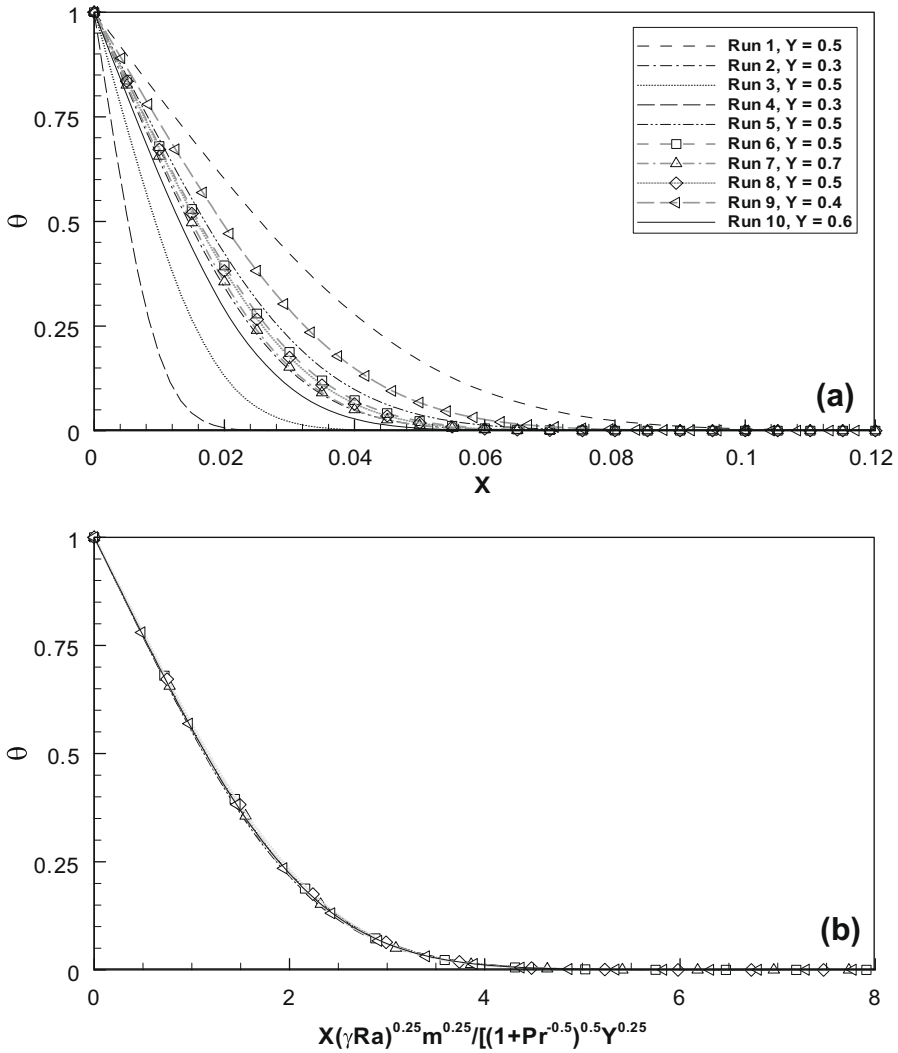

Fig. 6. Horizontal temperature profiles for all cases considered at different heights at steady state: (a) raw data and (b) θ plotted agains $X(\gamma Ra)^{0.25} m^{0.25} / [(1 + \mathrm{Pr}^{-0.5})^{0.5} Y^{0.25}]$.

$$\frac{\partial V}{\partial \tau}+U\frac{\partial V}{\partial X}+V\frac{\partial V}{\partial Y}=-\frac{\partial P}{\partial Y}+\frac{Pr}{(\gamma Ra)^{0.5}}\left(\frac{\partial^2 V}{\partial X^2}+\frac{\partial^2 V}{\partial Y^2}\right)-\frac{mPr}{2}\theta \tag{53}$$

$$\frac{\partial \theta}{\partial \tau}+U\frac{\partial \theta}{\partial X}+V\frac{\partial \theta}{\partial Y}=\frac{1}{(\gamma Ra)^{0.5}}\left(\frac{\partial^2 \theta}{\partial X^2}+\frac{\partial^2 \theta}{\partial Y^2}\right) \tag{54}$$

Where X, Y, U, V, θ, P, and τ are, respectively, the dimensionless forms of x, y, u, v, T, p, and t, which are made dimensionless by their respective characteristic scales, i.e.,

$$X=\frac{x}{H},\ Y=\frac{y}{H},\ U=\frac{u}{v_0},\ V=\frac{v}{v_0},\ \tau=\frac{t}{(H/v_0)},$$
$$P=\frac{p}{\rho v_0^2},\ \theta=\frac{T-T_0}{T_w-T_0}$$

The appropriate initial and boundary conditions for the system depicted in Fig. 1 are as follows:

$$U=V=0,\ \theta=0 \quad \text{at all } X, Y \text{ at } \tau<0,$$

and at $\tau \geqslant 0$:

$$U=V=0,\ \theta=1 \quad \text{at } X=0,$$
$$\frac{\partial U}{\partial X}=\frac{\partial V}{\partial X}=0,\ \frac{\partial \theta}{\partial X}=0 \quad \text{at } X=1,$$
$$U=V=0,\ \frac{\partial \theta}{\partial Y}=0 \quad \text{at } Y=0,1$$

5.1. Start-up stage scalings

The scaling relations can be now made dimensionless using H and v_0. During the start-up stage of the boundary-layer development, the scaling relations (22), (34), (35), (37) and (38) can be written in dimensionless form as:

$$\Delta_T=\frac{\delta_T}{H}\sim\frac{\kappa^{0.5}t^{0.5}}{H}\sim\frac{\tau^{0.5}}{(\gamma Ra)^{0.25}} \tag{55}$$

$$\Delta_v=\frac{\delta_v}{H}\sim\frac{v^{0.5}t^{0.5}}{H}\sim\frac{Pr^{0.5}\tau^{0.5}}{(\gamma Ra)^{0.25}} \tag{56}$$

$$\Delta_{vm}=\frac{\delta_{vm}}{H}\sim\frac{1}{1+Pr^{-0.5}}\frac{\kappa^{0.5}t^{0.5}}{H}\sim\frac{1}{1+Pr^{-0.5}}\frac{\tau^{0.5}}{(\gamma Ra)^{0.25}} \tag{57}$$

$$V_m=\frac{v_m}{v_0}\sim\gamma Ra\frac{m\kappa^2}{H^3}\left(\frac{1}{1+Pr^{-0.5}}\right)^2\frac{t}{v_0}\sim\frac{\tau m}{(1+Pr^{-0.5})^2} \tag{58}$$

$$Nu_Y\sim\frac{(\gamma Ra)^{0.25}}{\tau^{0.5}} \tag{59a}$$

$$Nu\sim\frac{1}{H}\int_0^H Nu_Y dY \tag{59a}$$

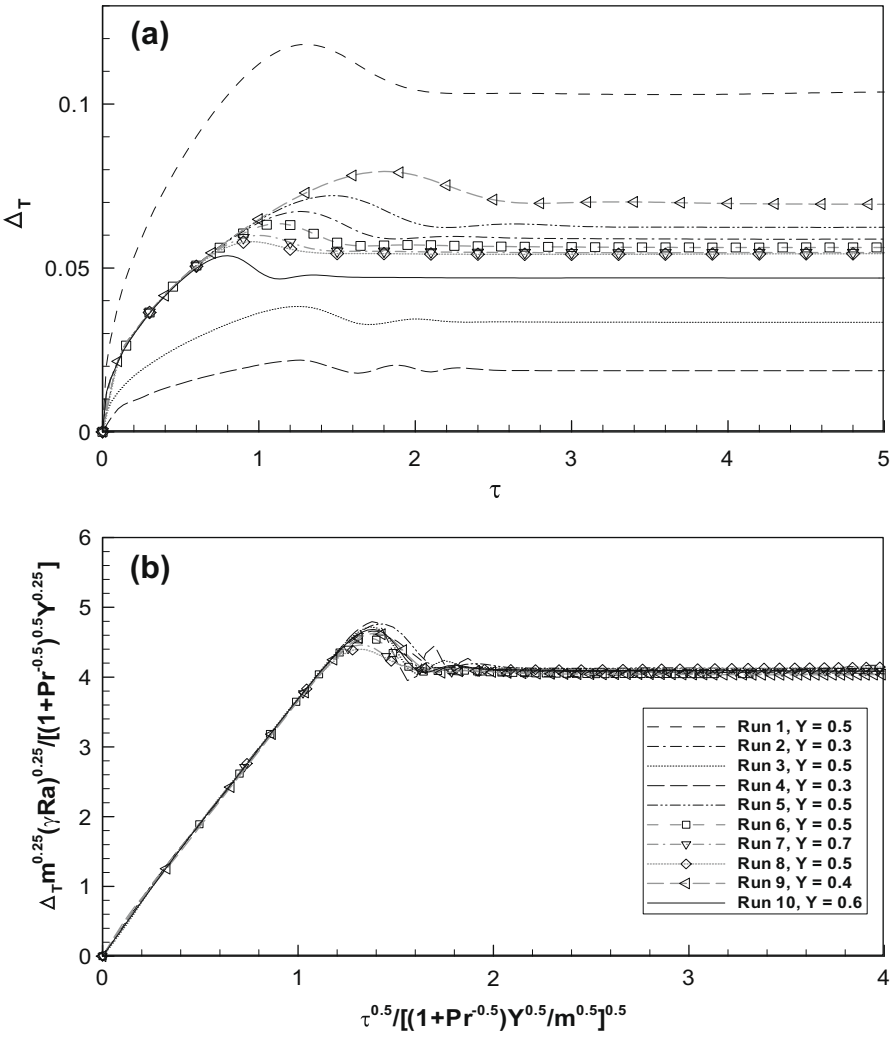

Fig. 7. Time series of Δ_T for all cases considered: (a) raw data and (b) $\Delta_T m^{0.25}(\gamma Ra)^{0.25}/[(1+\mathrm{Pr}^{-0.5})^{0.5}Y^{0.25}]$ plotted against $\tau^{0.5}/[(1+\mathrm{Pr}^{-0.5})Y^{0.5}/m^{0.5}]^{0.5}$.

5.2. Steady stage scalings

The dimensionless form of the scaling (43) for t_s is,

$$\tau_s = \frac{t_s}{(H/v_0)} \sim \frac{H^2}{(H/v_0)(\gamma Ra)^{0.5} m^{0.5} \kappa} \left(\frac{y}{H}\right)^{0.5} (1 + Pr^{-0.5}) \sim m^{-0.5}(1 + Pr^{-0.5})\, Y^{0.5} \tag{60}$$

The steady state scaling relations of the boundary-layer in dimensionless form, from (45), (46), (47), and (44), respectively, can be rewritten as follows:

$$\Delta_{T,s} = \frac{\delta_{T,s}}{H} \sim \frac{m^{-0.25}}{(\gamma Ra)^{0.25}} (1 + Pr^{-0.5})^{0.5} Y^{0.25} \tag{61}$$

$$\Delta_{v,s} = \frac{\delta_{v,s}}{H} \sim \frac{m^{-0.25}}{(\gamma Ra)^{0.25}} Pr^{0.5} (1 + Pr^{-0.5})^{0.5} Y^{0.25} \tag{62}$$

$$\Delta_{vm,s} = \frac{\delta_{vm,s}}{H} \sim \frac{m^{-0.25}}{(\gamma Ra)^{0.25}} (1 + Pr^{-0.5})^{-0.5} Y^{0.25} \tag{63}$$

$$V_{m,s} = \frac{v_{m,s}}{v_0} \sim \frac{m^{0.5}}{(1 + Pr^{-0.5})} Y^{0.5} \tag{64}$$

$$Nu_{s,Y} \sim \frac{(\gamma Ra)^{0.25} m^{0.25}}{Y^{0.25}} \frac{1}{(1 + Pr^{-0.5})^{0.5}} \tag{65}$$

$$Nu_s \sim \frac{(\gamma Ra)^{0.25} m^{0.25}}{(1 + Pr^{-0.5})^{0.5}} \tag{66}$$

Eqs. (55)–(57) clearly show that during the start-up stage, the boundary-layer development on the vertical wall is one-dimensional and independent of Y due to the dominance of pure conduction.

At the steady-state stage however, the boundary-layer development and the heat transfer across the vertical sidewall becomes two-dimensional, as shown by (61)–(66) due to domination of magnetic convection in the flow.

6. Numerical method and cases considered

Table 2 lists values of (γRa), Pr, and m for 10 simulation runs with selected values in the ranges $10^6 \leqslant (\gamma Ra) \leqslant 10^9$, $5 \leqslant Pr \leqslant 100$ and $1 \leqslant m \leqslant 5$.

The scaling predictions for magnetic convection of paramagnetic fluids obtained above are validated and analysed by numerical simulations with a double precision solver. The Eqs.

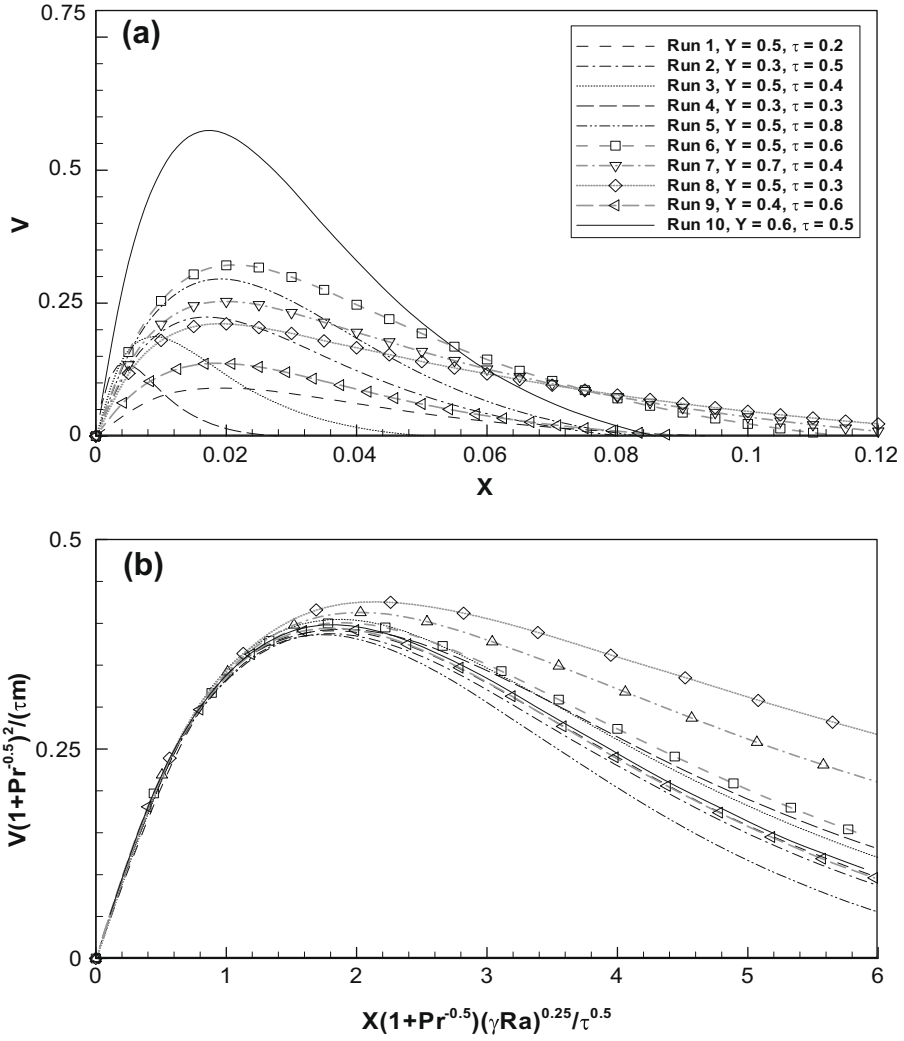

Fig. 8. Horizontal profiles of the vertical velocity for all cases considered at different heights and times during the start-up stage: (a) raw data and (b) $V(1 + \mathrm{Pr}^{-0.5})^2/(m\tau)$ plotted against $X(1 + \mathrm{Pr}^{-0.5})(\gamma Ra)^{0.25}/\tau^{0.5}$.

(51)–(54) are approximated with finite difference equations and the Highly Simplified Marker and Cell (HSMAC) method (Hirt et al., 1975) is used to simultaneously iterate the pressure and velocity fields on a staggered mesh/grid allocation system. The inertial terms in the momentum equations are approximated with a third-order upwind UTOPIA scheme (Tagawa and Ozoe, 1996). The absolute convergence criteria for the numerical solutions are specified based on the residual sums of all conserved quantities. If the residual sum is less than 10^{-6} for each conserved quantity, the equations are deemed to have converged at a specific time-step. The time-step is chosen to ensure numerical stability according to the Courant–Friedrichs–Lews (CFL) condition and is fixed at $\Delta\tau = 10^{-5}$ in all subsequent numerical simulations. The CFL number provides an indication of numerical stability and accuracy, and here it is kept less than one. More discussion of the CFL number effect can be found in Poinsot and Candel (1986).

The numerical methods used in this work for the simulation of thermo-magnetic convection have been widely verified by our group and/or co-workers, in both numerical and experimental investigations for closely related problems (Ozoe, 2005; Tagawa et al., 2002, 2003; Bednarz et al., 2004, 2005a,b, 2006, 2008, 2009; Kaneda et al., 2002; Tagawa and Ozoe, 1996), and therefore will not be repeated here.

The grid-dependency test is carried out to ensure that the simulation results are mesh-independent. A sample test has been conducted for Case 2 for which $\gamma Ra = 10^7$, $Pr = 10$, and $m = 2$. Fig. 4 presents numerically simulated horizontal profiles of temperature and vertical velocity at height $Y = 0.5$ at two different time instants: the $\tau = 0.5$ instant when the boundary-layer development is at the transitional stage, and the $\tau = 5.0$ instant at steady state. It is clearly demonstrated that the results are mesh-independent. Therefore, the medium mesh (251×251) is adopted in the present computations as a satisfactory compromise between numerical accuracy and the computing time.

7. Numerical results

As shown by the scaling relation (55), the dimensionless thermal boundary layer thickness, ρ_T, grows as $\Delta_T \sim \tau^{0.5}/(\gamma Ra)^{0.25}$ during the start-up stage, and shows no dependence on Pr, m nor Y. This is clearly confirmed by numerical results, as depicted in Fig. 5, where the horizontal temperature profiles for all cases considered are presented for different heights and times during the start-up stage. Fig. 5a shows the unscaled results, whereas Fig. 5b, where X is scaled by $\tau^{0.5}/(\gamma Ra)^{0.25}$, shows that this scale

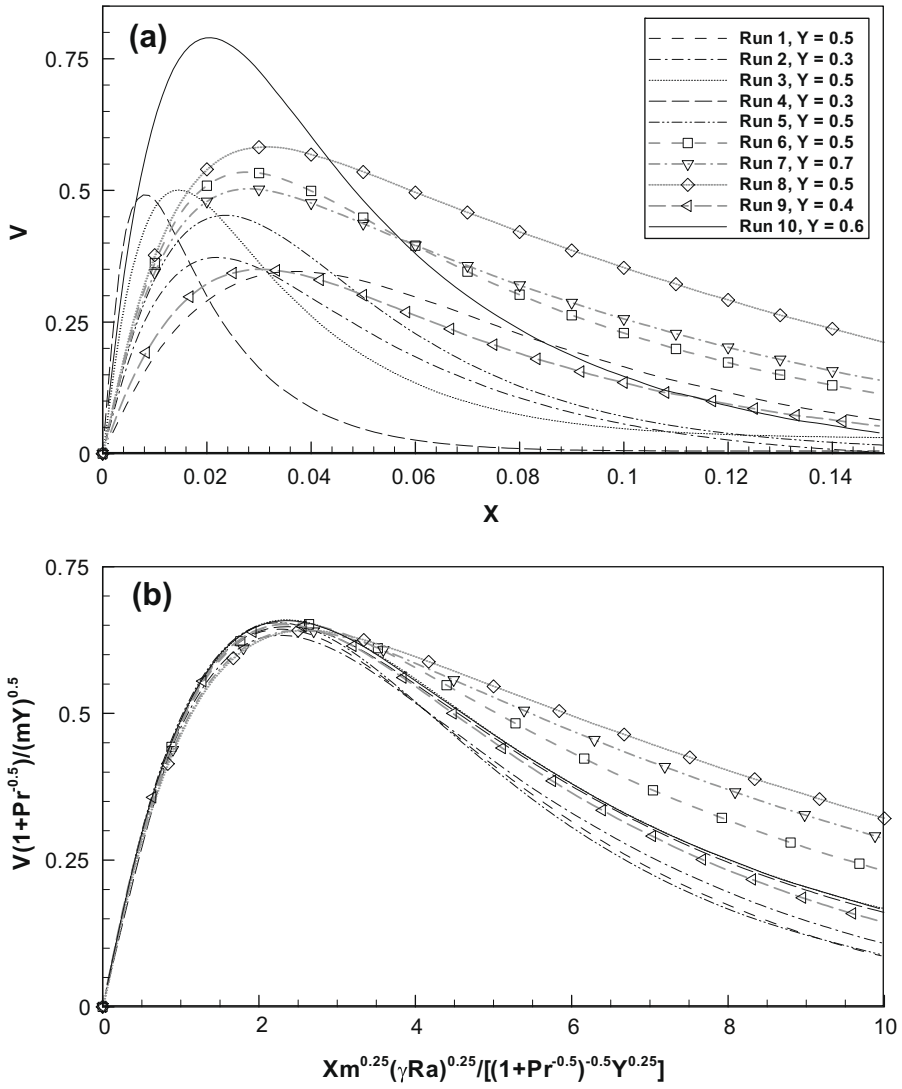

Fig. 9. Horizontal profiles of the vertical velocity for all cases considered at different heights at steady state: (a) raw data and (b) $V(1+\mathrm{Pr}^{-0.5})/(mY)^{0.5}$ plotted against $Xm^{0.25}(\gamma Ra)^{0.25}/[(1+\mathrm{Pr}^{-0.5})^{-0.5}Y^{0.25}]$.

brings all 10 scaled temperature profiles with varying (γRa), Pr, m and Y at different times into a single line, clearly demonstrating that $\Delta_T \sim \tau^{0.5}/(\gamma Ra)^{0.25}$ is the correct scaling for ρ_T at the start-up stage.

When the boundary-layer development attains steady state, the scaling (61) shows that the boundary layer becomes two-dimensional and the dimensionless thermal boundary layer thickness, $\rho_{T,s}$, becomes (γRa), Pr, m and Y dependent. This scaling is also confirmed by the numerical results, as shown in Fig. 6, where the horizontal temperature profiles at steady state for all cases considered are presented in Fig. 6a. Fig. 6b, where X is scaled by $(1+\mathrm{Pr}^{-0.5})^{0.5}Y^{0.25}/[(\gamma Ra)^{0.25}m^{0.25}]$, which is the scale for $\rho_{T,s}$ at steady state, shows that this scale also brings all 10 scaled temperature profiles with varying (γRa), Pr, m and Y at steady state onto a single line, confirming that the scaling (61) is the correct scaling for $\rho_{T,s}$ at steady state.

To more explicitly validate scaling relations (55), (60), and (61), the time series of ρ_T for varying (γRa), Pr, m and Y have been obtained from numerical simulations and are presented in Fig. 7. The value of ρ_T at a specific height is determined in the simulations as the distance from the vertical sidewall to the location where the dimensionless temperature θ of fluid becomes 0.01. The raw data obtained from the 10 numerical runs is shown in Fig. 7a and b presents the same 10 time series as those shown in Fig. 7a, but with ρ_T and τ scaled, respectively, by $(1+\mathrm{Pr}^{-0.5})^{0.5}Y^{0.25}/[(\gamma Ra)^{0.25}m^{0.25}]$ and $(1+\mathrm{Pr}^{-0.5})Y^{0.5}/m^{0.5}$. These are the scales for $\rho_{T,s}$ and τ_s at steady state, respectively, as shown by scaling relations (60) and (61). At the start-up stage (before each series attains its individual peak), it is seen that all 10 scaled series (with varying (γRa), Pr, m and Y) lie on the same straight line, again confirming that $\Delta_T \sim \tau^{0.5}/(\gamma Ra)^{0.25}$ is the correct scaling for ρ_T at the start-up stage. At steady state, these scaled series lie approximately on the same horizontal straight line, which clearly confirms that $\Delta_{T,s} \sim (1+\mathrm{Pr}^{-0.5})^{0.5}Y^{0.25}/[(\gamma Ra)^{0.25}m^{0.25}]$ is the correct scaling for $\rho_{T,s}$ at steady state. Additionally, Fig. 7b shows that all 10 scaled series attain their respective peaks almost at the same scaled time with acceptable deviations, also validating scaling relation (60).

Scaling relation (57) predicts that during the start-up stage, the inner viscous boundary layer thickness ρ_{vm} is dependent upon (γRa) and Pr but independent of y and m, whereas scaling relation (58) predicts that during this stage the maximum vertical velocity, $V_{m,}$ is dependent upon Pr and m but independent of y and (γRa). These scalings have been validated with the numerical results shown in Fig. 8, in which the horizontal profiles of the vertical velocity at different heights and times during the start-up stage are shown for all cases in Fig. 8a. In Fig. 8b, V and X are scaled, respectively, by $m\tau/(1+\mathrm{Pr}^{-0.5})^2$ and $\tau^{0.5}/[(1+\mathrm{Pr}^{-0.5})(\gamma Ra)^{0.25}]$ which are the scales for V_m and ρ_{vm} at the start-up stage. It is seen

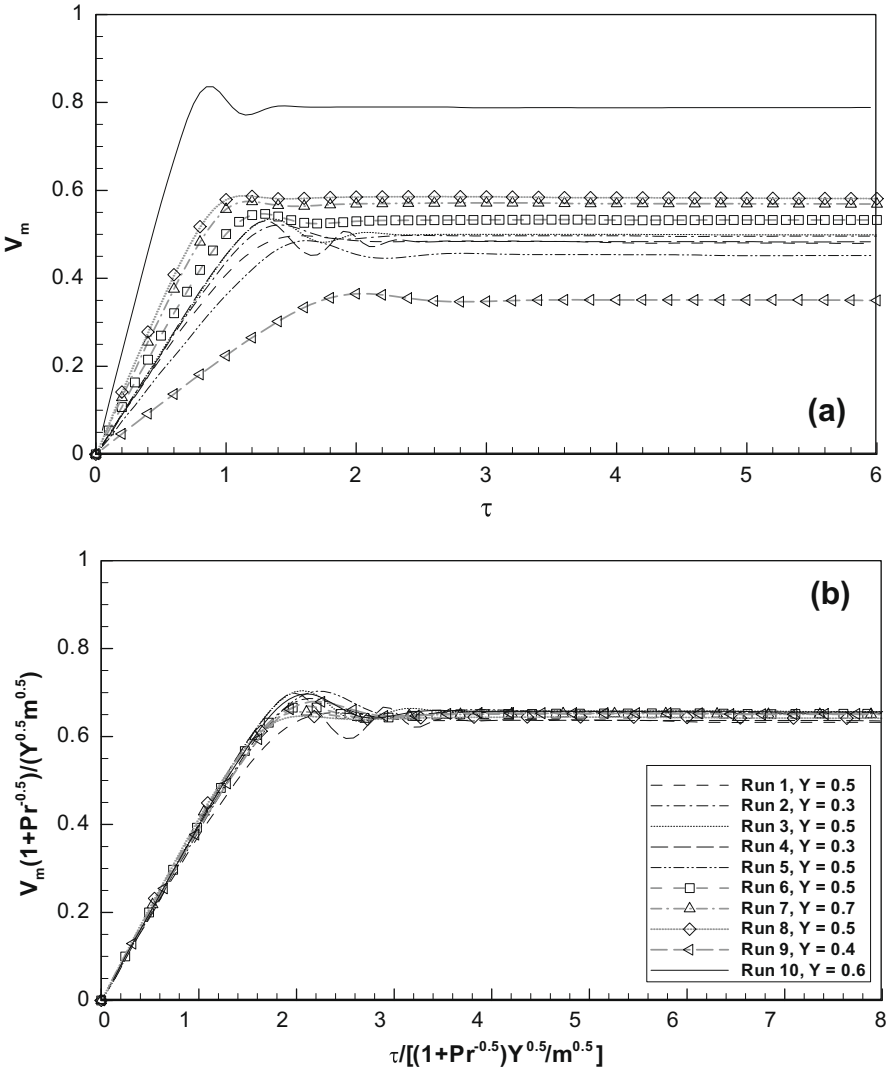

Fig. 10. Time series of V_m for all cases considered: (a) raw data and (b) $V_m/(1+\mathrm{Pr}^{-0.5})/(Y^{0.5}m^{0.5})$ plotted against $\tau/[(1+\mathrm{Pr}^{-0.5})Y^{0.5}/m^{0.5}]$.

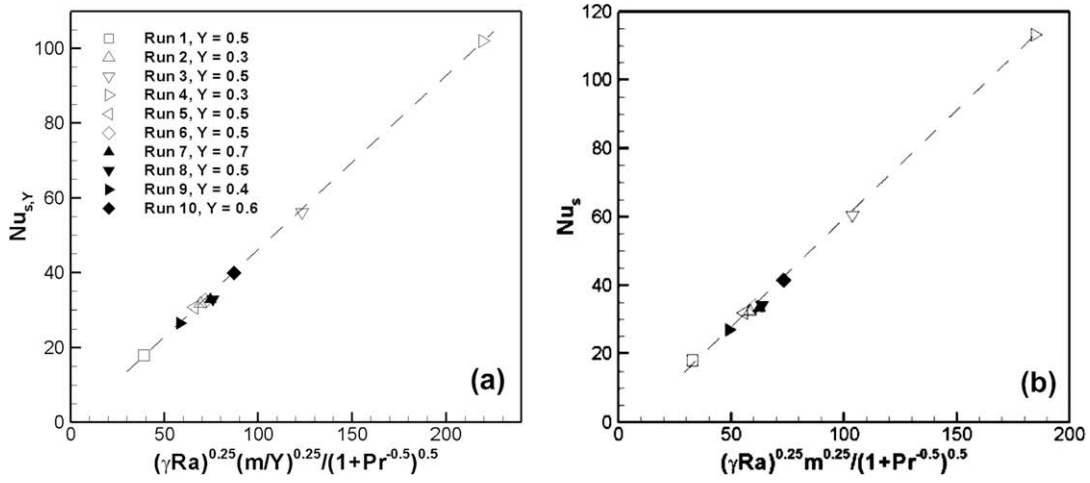

Fig. 11. (a) $Nu_{s,Y}$ plotted against $\frac{(\gamma Ra)^{0.25}m^{0.25}}{Y^{0.25}}\frac{1}{(1+Pr^{-0.5})^{0.5}}$ for all cases considered and (b) Nu_s plotted against $\frac{(\gamma Ra)^{0.25}m^{0.25}}{(1+Pr^{-0.5})^{0.5}}$ for all cases considered. Dashed lines represent linear trend lines.

that these two scales bring all 10 scaled profiles within the inner viscous boundary layers into a single line at the start-up stage, clearly validating scalings (57) and (58).

At steady state, the viscous boundary layer also becomes two-dimensional and dependent upon (γRa), Pr and m, as indicated by scaling relations (63) and (64). These are also validated by the numerical results shown in Fig. 9, in which the horizontal profiles of the vertical velocity at steady state for all cases are shown in Fig. 9a. In Fig. 9b the scaled profiles are presented with V and X scaled, respectively, by $m^{0.5}Y^{0.5}/(1+\mathrm{Pr}^{-0.5})$ and $(1+\mathrm{Pr}^{-0.5})^{-0.5}Y^{0.25}/[m^{0.25}(\gamma Ra)^{0.25}]$, which are the scales for $V_{m,s}$ and $\rho_{vm,s}$ at steady state. It is clearly seen that these two scales bring all 10 scaled profiles within the inner viscous boundary layers onto a single line at steady state, confirming scalings (63) and (64).

Fig. 10 presents further numerical results to validate scalings (57), (63), and (60), in which the time series of V_m for varying (γRa), Pr, m and Y are presented in Fig. 10a. Fig. 10b presents the same 10 time series as those present in Fig. 10a, but with V_m and τ scaled, respectively, by $m^{0.5}Y^{0.5}/(1+\mathrm{Pr}^{-0.5})$ and $(1+\mathrm{Pr}^{-0.5})Y^{0.5}/m^{0.5}$. These are the scales for $V_{m,s}$ and τ_s at steady state, respectively, as shown by the scalings (60) and (64). It is found that all 10 scaled time series line approximately on the same straight line for the start-up stage, confirming that $V_m \sim m\tau/(1+\mathrm{Pr}^{-0.5})^2$ is the correct scaling relation for V_m during the start-up stage. At steady state, it is seen that all scaled time series line essentially on the same horizontal straight line, clearly confirming that $V_{m,s} \sim m^{0.5}Y^{0.5}/(1+\mathrm{Pr}^{-0.5})$ is the correct scaling for $V_{m,s}$ at steady state. Additionally, Fig. 10b shows that all 10 scaled time series attain their respective peaks almost at the same scaled time, also validating scaling relation (60).

Fig. 11 presents the numerical results for both the local and global Nusselt numbers at steady state for all cases considered. From Fig. 11a, it is seen that the scale $(\gamma Ra)^{0.25}m^{0.25}/[Y^{0.25}(1+\mathrm{Pr}^{-0.5})^{0.5}]$ collapses all values of $Nu_{s,Y}$ onto the same straight line, clearly demonstrating that $Nu_{s,Y}$ scales with $(\gamma Ra)^{0.25}m^{0.25}/[Y^{0.25}(1+\mathrm{Pr}^{-0.5})^{0.5}]$ and confirms scaling relation (65). Similarly, it is seen from Fig. 11b that the scale $(\gamma Ra)^{0.25}m^{0.25}/[(1+\mathrm{Pr}^{-0.5})^{0.5}]$ collapses all values of Nu_s onto the same straight line, clearly demonstrating that Nu_s scales with $(\gamma Ra)^{0.25}m^{0.25}/[Y^{0.25}(1+\mathrm{Pr}^{-0.5})^{0.5}]$ and confirms scaling (66).

8. Conclusions

Thermo-magnetic boundary-layer development in a two-dimensional open squared cavity filled with a paramagnetic fluid of $Pr > 1$ and subject to a gradient magnetic field is predicted using a scaling analysis. The verification of the scaling relations includes thermal and viscous boundary-layer developments as well as the heat transfer rate predictions. Numerical results demonstrate that the scalings accurately represent the physical behaviour of the whole stage of the flow development. The present scaling analysis incorporates a three-region structure for the boundary layer that improves scaling predictions especially where the Pr variation effect is taken into account. It is clearly shown by scaling and verified by numerical simulations that during the start-up stage the boundary-layer development is one-dimensional, independent of height, and becomes two-dimensional and height dependent when the convection starts to dominate the flow.

Acknowledgments

Many thanks go to Prof. Hiroyuki Ozoe and Dr. John Malos for their constructive comments on the last version of this paper.

References

Aberra, T. Armfield, S.W. Behnia, M., 2008. Prandtl number scaling of the natural convection flow over an evenly heated vertical plate ($Pr > 1$).In: Proceedings of CHT-08, ICHMT International Symposium on Advances in Computational Heat Transfer, vol. 13, Paper No CHT-8-363.

Armfield, S.W., Patterson, J.C., Lin, W., 2007. Scaling investigation of the natural convection boundary layer on an evenly heated plate. International Journal of Heat and Mass Transfer 50, 1592–1602.

Bai, B., Yabe, A., Qi, J., Wakayama, N.I., 1999. Quantitative analysis of air convection caused by magnetic-fluid coupling. AIAA Journal 37 (12), 1538–1543.

Bednarz, T., Tagawa, T., Kaneda, M., Ozoe, H., 2004. Magnetic and gravitational convection of air with a coil inclined around the X axis. Numerical Heat Transfer, Part A 46, 99–113.

Bednarz, T., Fornalik, E., Tagawa, T., Ozoe, H., Szmyd, J.S., 2005a. Experimental and numerical analyses of magnetic convection of paramagnetic fluid in a cube heated and cooled from opposing vertical walls. International Journal of Thermal Sciences 44, 933–943.

Bednarz, T., Tagawa, T., Kaneda, M., Ozoe, H., Szmyd, J.S., 2005b. The convection of air in a cubic enclosure with an electric coil inclined in general orientations. Fluid Dynamics Research 36, 91–106.

Bednarz, T., Fornalik, E., Tagawa, T., Ozoe, H., Szmyd, J.S., 2006. Convection of paramagnetic fluid in a cube heated and cooled from side walls and placed below a superconducting magnet – comparison between experiment and numerical computations. Thermal Science & Engineering Journal 14, 107–114.

Bednarz, T., Fornalik, E., Ozoe, H., Szmyd, J.S., Patterson, J.C., Lei, C., 2008. Influence of a horizontal magnetic field on the natural convection of paramagnetic fluid in a cube heated and cooled from two vertical side walls. International Journal of Thermal Science 47, 669–679.

Bednarz, T. Lei, C. Patterson, J.C. Ozoe, H., 2009. Effects of a transverse, horizontal magnetic field on natural convection of a paramagnetic fluid in a cube. International Journal of Thermal Sciences 48, 26–33.

Braithwaite, D., Beaugnon, E., Tournier, R., 1991. Magnetically controlled convection in paramagnetic fluid. Nature 354, 667–673.

Carruthers, J.R., Wolfe, R., 1968. Magnetothermal convection in insulating paramagnetic fluids. Journal of Applied Physics 39, 5718–5722.
Chandrasekhar, S., 1981. Hydrodynamics and Hydromagnetic Stability. Dover Publishing Inc., New York.
CRC Handbook of Chemistry and Physics, 88th ed. CRC Press, Boca Raton, FL, 2007–2008.
Hirt, C.W. Nichols, B.D. Romero, N., 1975. A numerical solution algorithm for transient fluid flow, Los Alamos Scientific Laboratory, LA-5852.
Kaneda, M., Tagawa, T., Ozoe, H., 2002. Convection induced by a cusp-shaped magnetic field for air in a cube heated from above and cooled from below. International Journal of Heat Transfer 124, 17–25.
Lin, W., Armfield, S.W., 1999. Direct simulation of natural convection cooling in a vertical cylinder. International Journal of Heat and Mass Transfer 42, 4117–4130.
Lin, W., Armfield, S.W., 2005. Long-term behaviour of cooling fluid in a vertical cylinder. International Journal of Heat and Mass Transfer 48, 53–66.
Lin, W., Armfield, S.W., Patterson, J.C., Lei, C., 2009. Prandtl number scaling of unsteady natural convection boundary layers for $Pr > 1$ fluids under isothermal heating. Physical Review E 79, Paper No 066313.
Lin, W., Armfield, S.W., Morgan, P.L., 2002. Unsteady natural convection boundary-layer flow along a vertical isothermal plate in a linearly stratified fluid with $Pr > 1$. International Journal of Heat and Mass Transfer 45, 451–459.
Lin, W., Armfield, S.W., Patterson, J.C., 2007. Cooling of a $Pr < 1$ fluid in a rectangular container. Journal of Fluid Mechanics 574, 85–108.
Lin, W., Armfield, S.W., Patterson, J.C., 2008. Unsteady natural convection boundary-layer flow of a linearly-stratified fluid with $Pr < 1$ on an evenly heated semi-infinite vertical plate. International Journal of Heat and Mass Transfer 51, 327–343.
Ozoe, H., 2005. Magnetic Convection. Imperial College Press (ISBN 1-86094-578-3).
Patterson, J.C., Armfield, S.W., 1990. Transient features of natural convection in a cavity. Journal of Fluid Mechanics 219, 469–497.
Patterson, J.C., Imberger, J., 1980. Unsteady natural convection in a rectangular cavity. Journal of Fluid Mechanics 100, 65–86.
Patterson, J.C., Lei, C., Armfield, S.W., Lin, W., 2009. Scaling of unsteady natural convection boundary layers from a non-instantaneous initiation. International Journal of Thermal Sciences 48, 1843–1852.
Poinsot, T., Candel, S.M., 1986. The influence of differencing and CFL number on implicit-dependant non-linear calculations. Journal of Computational Physics 62, 282–296.
Schlichting, H., Gersten, K., 2000. Boundary Layer Theory. Springer-Verlag, Berlin Heidelberg.
Shigemitsu, R., Tagawa, T., Ozoe, H., 2003. Numerical computation for natural convection of air in a cubic enclosure under combination of magnetizing and gravitational forces. Numerical Heat Transfer, Part A 43, 449–463.
Tagawa, T., Ozoe, H., 1996. Effect of Prandtl number and computational schemes on the oscillatory natural convection in an enclosure. Numerical Heat Transfer A 30, 271–282.
Tagawa, T., Shigemitsu, R., Ozoe, H., 2002. Magnetizing force modelled and numerically solved for natural convection of air in a cubic enclosure: effect of the direction of the magnetic field. International Journal of Heat and Mass Transfer 45, 267–277.
Tagawa, T., Ujihara, A., Ozoe, H., 2003. Numerical computation for Rayleigh-Benard convection of water in a magnetic field. International Journal of Heat and Mass Transfer 46, 4097–4104.